

## Estimating location and size of historical earthquake by combining archaeology and geology in Umm-El-Qanatir, Dead Sea Transform

Neta Wechsler · Oded Katz · Yehoshua Dray · Ilana Gonen · Shmuel Marco

Received: 7 July 2008 / Accepted: 28 October 2008  
© Springer Science+Business Media B.V. 2008

**Abstract** We study the Byzantine-to-Umayyad (6th–8th century) archaeological site of Umm-El-Qanatir, located 10 km east of the Dead Sea Transform (DST) in northern Israel. The site was damaged by an earthquake-induced landslide, and in this work we use slope stability analysis to constrain the historical seismic acceleration that occurred along the northern segment of the DST. Umm-El-Qanatir archaeological site is located on a slope of a canyon and contains evidence for earthquake-related damage, including fallen columns and walls, horizontal shift of heavy masonry blocks, and complete burial of ceramic pots and farming tools beneath fallen ceilings. A water pool that collected spring water is displaced nearly one meter by the landslide. The artifacts from the village and the spring area indicate that people inhabited the site until the middle of the 8th century. We argue that the destruction, which forced the abandonment of Umm-El-Qanatir together with nearby settlements, was associated with the earthquake of January 18, 749 CE. In order to evaluate the ground acceleration related to the above earthquake, we back-analyze the stability of a failed slope, which cut and displaced the water-pool, using slope stability software (Slope/W). The results show that the slope is statically stable and that high values of horizontal seismic acceleration ( $>0.3$  g) are required to induce slope failure. Subsequently, we use the Newmark displacement method to calculate the earthquake magnitude

---

N. Wechsler (✉) · S. Marco  
Department of Geophysics and Planetary Sciences, Tel Aviv University, Tel Aviv, Israel  
e-mail: wechsler@usc.edu

S. Marco  
e-mail: shmulikm@post.tau.ac.il

*Present Address:*  
N. Wechsler  
Department of Earth Sciences, University of Southern California, Los Angeles, CA, USA

O. Katz  
Geological Survey of Israel, Jerusalem, Israel  
e-mail: odedk@gsi.gov.il

Y. Dray · I. Gonen  
Restoration of Ancient Technology, Binyamina, Israel

needed to cause the slope failure as a function of distance from the site. The results (attributed to the 749 CE earthquake) show that a  $M_w > 7.0$  earthquake up to 25 km from the site could have induced the studied landslide.

**Keywords** Dead-Sea transform · Historical earthquakes · Landslides · Archaeoseismology · Peak ground acceleration

## 1 Introduction

Information on past earthquakes significantly contributes to the understanding of seismic activity and seismic hazard. However, historical accounts are often hard to interpret or translate into modern terms because they might be vague, incomplete, biased, exaggerated, or inaccurate. Being unaware of faulting as part of the earthquake process, the historians documented primarily damage to settlements with only minor attention to natural phenomena. Consequently, the recovery of earthquake source faults and the size of past earthquakes are usually achieved through complementary paleoseismic and archaeoseismic studies, which can give better quantitative estimations of earthquake locations, magnitudes, and timing.

Historical records attest to the occurrence of moderate to strong earthquakes along the Dead Sea Transform (DST). Many of these earthquakes, which caused extensive damage to settlements, were recorded by contemporaries and catalogued by recent scholars (e.g., Amiran et al. 1994; Guidoboni and Comastri 2005; Guidoboni et al. 1994; Sbeinati et al. 2005). Many of the damaged structures are still preserved throughout the region (Marco 2008). Albeit important, historical records and archaeological findings provide only rough estimation on the locations and magnitudes of their associated earthquakes. In this study, we show how archaeology, history, geology, and engineering-geology can be combined to constrain the location and magnitude of a historical earthquake, which cannot be inferred from the historical records alone. We analyze a case of the recently excavated Umm-El-Qanatir (Arabic, “Mother of Arches”) Byzantine archaeological site (Table 1), located 10 km east of the DST eastern boundary fault, in the vicinity of the Sea of Galilee (Fig. 1). We present evidence that the site was apparently damaged by an earthquake-induced landslide. We use the damage to the archaeological structures to constrain the landslide geometry, and then perform a slope stability analysis to constrain the causative seismic-acceleration. Archaeological stratigraphy and historical information are applied for dating the damaging earthquake.

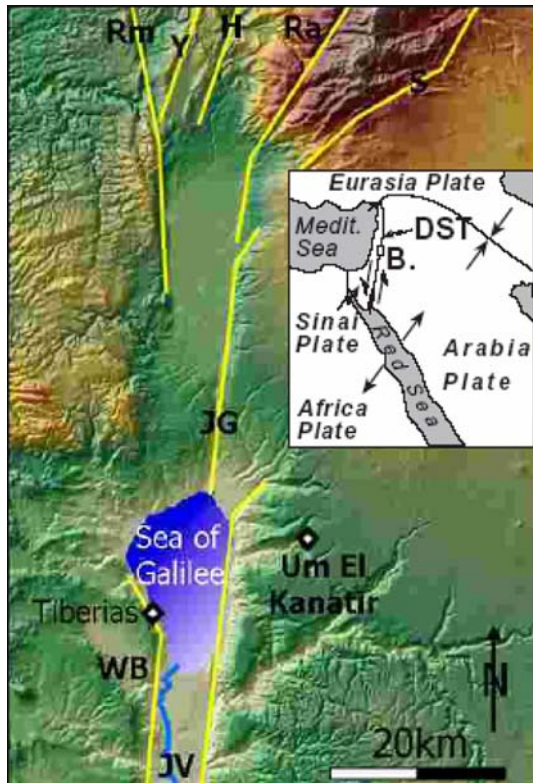
### 1.1 Geology

The study area is located on the eastern margin of the DST, a sinistral fault which transfers the opening in the Red-Sea to the collision in the Taurus and Zagros Mountains (Fig. 1).

**Table 1** Historical periods in the Middle-East

Period	Dates
Roman	37 BCE to 324 CE
Byzantine	324 CE to 638 CE
Early Arabic—Ummayad	638 CE to 750 CE
Early Arabic—Abassid	750 CE to 1099 CE
Arabic and Crusader	1099 CE to 1291 CE

**Fig. 1** Location map of the study area based on a DEM of the Sea of Galilee region, a pull-apart basin along the DST. Shaded relief from Hall (1994). Active faults are yellow. The DST main branch is the Yammouneh Fault (labeled Y). Other fault branches that splay off the main one are Roun (Rm), Hazbaya (H), Rashaya (Ra), and Sergahaya (S). JV = Jordan Valley Fault, WB = Western Boundary Fault, JG = Jordan Gorge Fault. Inset shows the plate tectonic setting of the Dead Sea Transform: a left lateral fault, which transfers the opening in the Red Sea to the collision between Arabia and Euroasia by northward movement of the Arabia plate with respect to the Sinai sub-plate



A cumulative offset of  $\sim 105$  km accommodates the relative northward movement of the Arabia plate with respect to the Sinai sub-plate since the Miocene (e.g., Freund et al. 1968; Garfunkel 1981).

Umm-El-Qanatir is an archeological site located in the southwestern part of the Golan Heights volcanic plateau, on the eastern bank of the northern tributary of Samak Creek (Fig. 1). Several transform-related secondary faults extend into the southern part of the Golan Heights, taking up some of the lateral and normal motion. The exposed stratigraphy of the area consists of the Miocene clastic Hordos Formation (mostly conglomerates and sandstones and some shales, marls, and limestone beds) overlain by a Pliocene Basalt called “Cover Basalt” (CB). The CB covers most of the southern Golan Heights and its flows are interbedded with layers of fossil clay-rich paleosols of various thicknesses (Michelson 1979). The study area is located above the contact of the CB with the Hordos Formation, where a thin (about 1 m thick) layer of reddish paleosol underlying the CB and forms the aquiclude for a perennial spring (Fig. 2). The CB (and the reddish paleosol) is covered in places by a layer of brown pedogenic soil with floating basaltic cobbles and pebbles, a soil that typically develops over basalts. In other places the basalt is exposed in the form of cliffs, sometimes with a columnar structure, especially at the creek margins. Grain size distribution following USCS procedure (ASTM 1985) of the brown soil (sample KA-2) and the reddish paleosol (sample KA-4) reveals that both are silty-clayey sands (SM-SC), with less than 5% carbonates (Fig. 3). The reddish paleosol consists of significant amount of silt and clay size grains (30–40%).

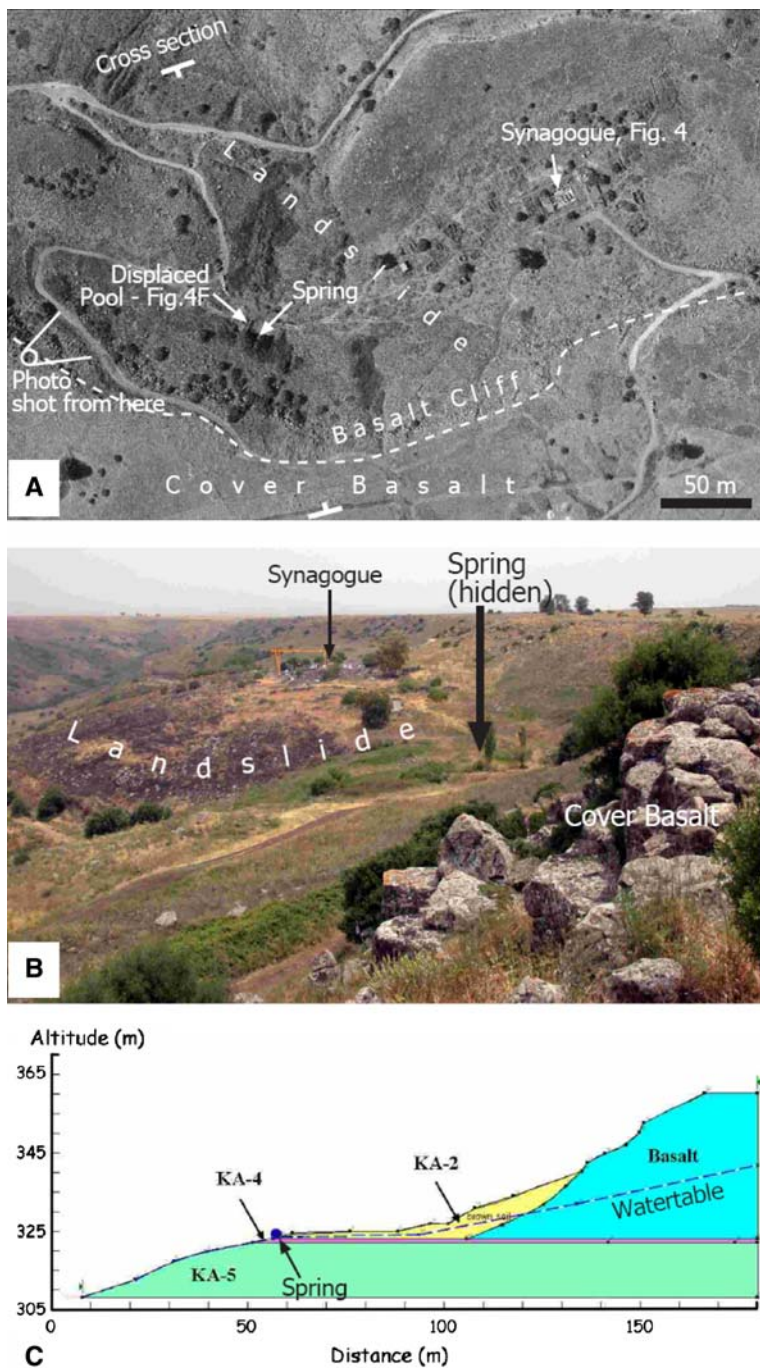
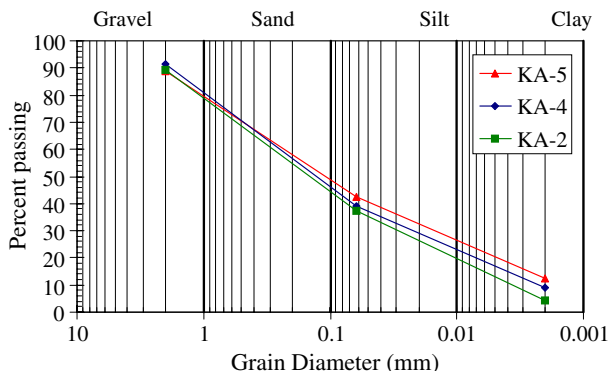


**Fig. 2** **a** Aerial photo of study area. **b** A northward look at the Umm-El-Qanatir site. **c** Cross section showing geological units and sample numbers. Watertable is assumed. This section is used to model slope stability and its trace is shown in the aerial photo (top)

**Fig. 3** Gradation curve (using USCS procedure; ASTM 1985) showing granulometry of the different tested soil samples (KA-2, KA-4, KA-5)



The reddish paleosol is underlaid by a dark gray layer (sample KA-5), of very similar composition (slightly more coarse grains, Fig. 3) but different in color. This layer may have formed by weathering of an unexposed basalt flow.

The existence of the year-round flowing spring (and several others in the vicinity) indicates a high water table, and the weather patterns (rainy winter with  $\sim 900$  mm average annual rainfall) suggest that at times it can be as high as the topography.

## 1.2 Seismicity

The DST is capable of producing large earthquakes, with magnitudes up to 7.5 (Begin et al. 2005). Damaging earthquakes on the DST in the section and the time relevant to our study occurred in 363, 747–9, 1033, 1202, 1759, and 1837 CE (Amiran et al. 1994; Guidoboni and Comastri 2005; Guidoboni et al. 1994). Of particular interest to our study are one or more earthquakes that affected the Levant during the period of 747 to 757 CE, hereafter referred to as the 749 event. The 749 earthquake almost totally destroyed the towns near the Sea of Galilee, Tiberias, Sussita (Hippos), and Bet Shean (Ambraseys 2005; Karcz 2004; Marco et al. 2003). Surface faulting dated to the 749 was found in archaeological excavations in Tiberias (Marco et al. 2003) and in paleoseismic trenches north of the Dead Sea (Reches and Hoexter 1981), indicating a magnitude of at least 7 for the earthquake rupture along the Jordan Valley. Displacements of archaeological walls and stream channels dated to the 1202 and the 1759 earthquakes were documented along the Jordan River, north of the Sea of Galilee (Daëron et al. 2005; Ellenblum et al. 1998; Marco et al. 2005).

## 2 Archaeological observations

The proximity of the archaeological site of Umm-El-Qanatir to the DST makes its structures a potential recorder of past earthquakes. Artifacts in Umm-El-Qanatir all date between the Byzantine and early Arabic periods (Table 1). Based on indicative artifacts, we conclude that the site has been abandoned since the middle of the 8th century. All the valuable meticulously carved masonry stones, almost invariably robbed from other sites in the region, were left in situ here. The structures in the site exhibit extensive typical seismogenic damage: displaced and cracked masonry stones, directional fall of walls, and sliding of arch stones (Fig. 4).

The Umm-El-Qanatir site comprises of two main parts, a village and a spring. The village includes several buildings, the largest of which is a  $14 \times 19$  m two-storey

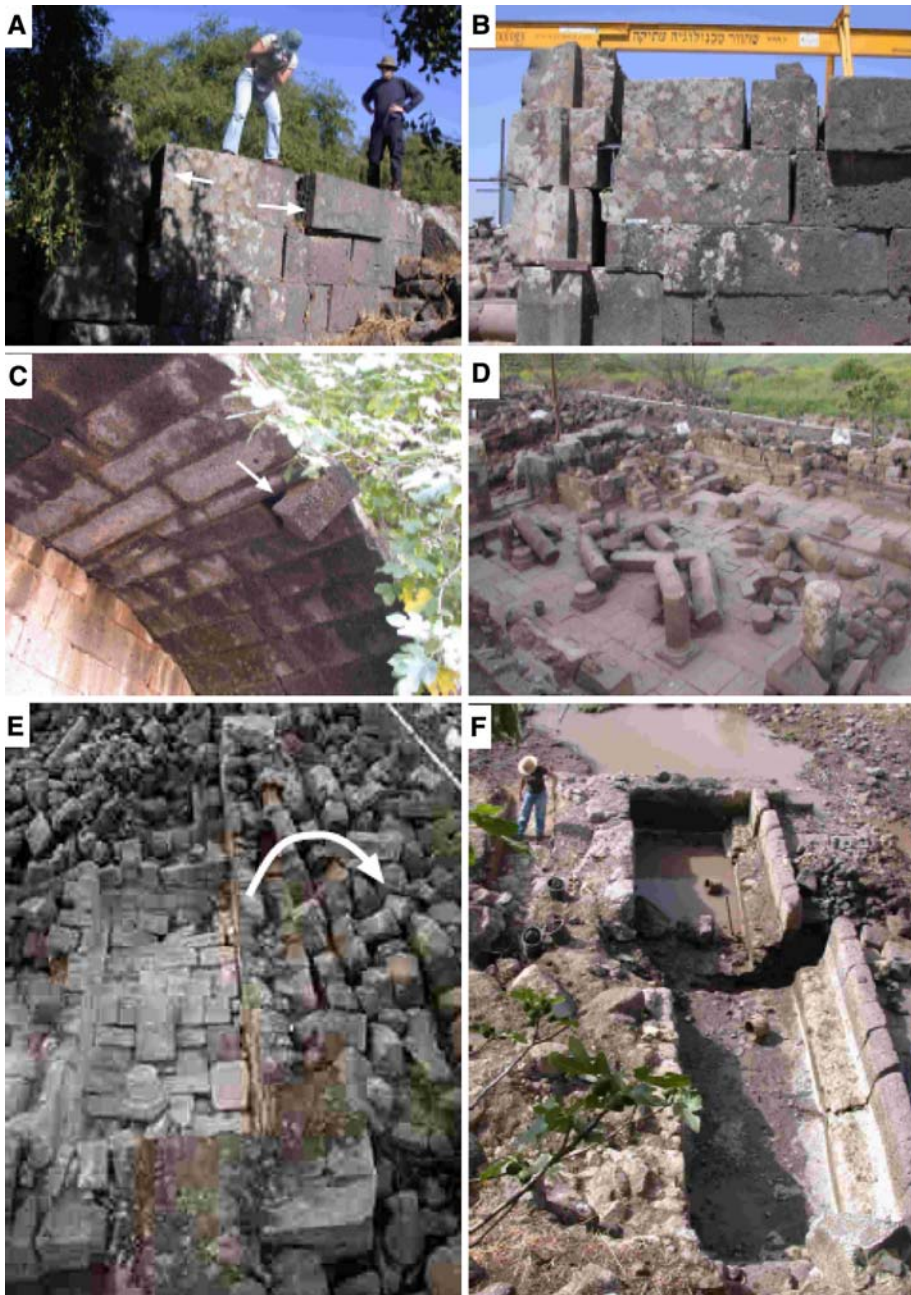


**Fig. 4** Earthquake induced damage to buildings in Umm-El-Qanatir. **a** and **b** Horizontal shift of a large masonry basalt blocks at the synagogue wall. **c** Keystones of an arch that slid out. **d** Aligned fallen columns. **e** Westward collapse of the wall of the synagogue. **f** A water pool, part of the spring complex, displaced laterally 95 cm. This water pool is displaced by the landslide and is used for the slope stability analysis

synagogue, one of the largest synagogues in the Golan area. It was discovered in 1884 by Schumacher and Oliphant (Oliphant 1886; Schumacher 1886) and later excavated for the first time by Kohl and Watzinger (1916), who drew the building's plan in details. All the above authors concluded that the building was ruined by an earthquake.

The western wall and most of the columns of the synagogue, collapsed westward (Fig. 4e). This direction is similar to the directional of fall of the columns in three basilicas at Sussita, an archaeological site about 10 km to the southwest of Umm-El-Qanatir, which was affected by one of the mid-8th century earthquakes (Segal et al. 2003). Other typical earthquake-triggered damage is the horizontal shift of the entrance pier and of large basalt blocks ( $\sim 1 \text{ m}^3$ ) in the southern wall of the synagogue (Fig. 4a, b). A small  $4 \times 6 \text{ m}$  makeshift house was found inside the synagogue (Fig. 5). It was built on the synagogue's tiled floor with many of the synagogue's recycled fancy stones, after the synagogue was damaged. Agricultural tools such as spades, hoes, and sickles, which were found below the rubble, indicate that this secondary building belonged to a farmer who took advantage of the ruined structure. It is highly unlikely that someone would build such a house while the synagogue was active. The farmer's house itself had collapsed and buried these useful artifacts, indicating a sudden, unexpected (second) disaster. The absences of artifacts that postdate the middle 8th century indicate that the site was abandoned, like other nearby settlements including Sussita, most likely because of the 749 CE earthquake. The neighboring larger towns of Tiberias and Bet Shean were rehabilitated after the earthquake. The accurate dating of archaeological artifacts of this period relies on dramatic



**Fig. 5** The synagogue suffered two damaging events. The first led to its abandonment, as evidenced by a makeshift house (marked with dashed line), which was built on the floor of the synagogue using many of its finely carved stones. The second event caused the destruction of this house and triggered the abandonment of the whole site, as evidenced by absence of post mid-8th century artifacts

changes in 750 CE, when the Abbassid Caliphate replaced the Umayyad Caliphate and moved the capital of the Arab Empire from Damascus to Baghdad.

The spring flows from an aquifer in the Cover Basalt, about 200 m south of the village. Its water were collected by a monumental structure consisting of three arches, a  $8.75 \times 2.22$  m, 1.2 m deep water pool, and several smaller pools connected by clay pipes. The character and size of the structure indicates its importance to the village denizens beyond a water source. It played an important part in the village's main industry of fine linen production. Two of the three arches are still beautifully preserved while the western one is half ruined. Typical earthquake damage to the spring area is apparent in the form of a tilted and broken pavement and a displacement of the water pool by a total of  $\sim 1$  m to left-laterally (Fig. 4f). The pottery shards unearthed from the pool all date up to mid-8th century. No post-8th century artifacts were found in the excavations, nor was the damaged pool ever fixed, suggesting that the site was abandoned at that time after sustaining serious damage, or that the damage occurred post-abandonment. In an exploratory trench dug where the water pool is broken we encountered the red clay layer of baked palesol (KA-2), typical of soils that are found throughout the Golan Heights between basalt flows. This impermeable layer is the aquiclude of the spring. The red clay exhibits continuous shearing where the pool is offset. The ancient masons built the pool directly on the red clay, taking advantage of its impermeability (Fig. 6).

Based on these observations, we argue that the cause of damage in the spring area is most probably an earthquake-induced landslide. This conclusion is based on the typical landslide morphology of the spring area—the slope is quite steep (up to  $40^\circ$ ) and its crescent shape is compatible with a slide scarp (Fig. 2a, b); on the weak geological material the site is founded on, which enables slope failure; and on the existing water at the slope surface (the spring) that also promotes slope failure.

We did not find any fault scarps in the area of the Umm-El-Qanatir site, the underlying strata are not faulted, and no active faults have been mapped in the site in previous surveys (Bartov et al. 2002). This further supports the landslide origin for the displacement of the pool.

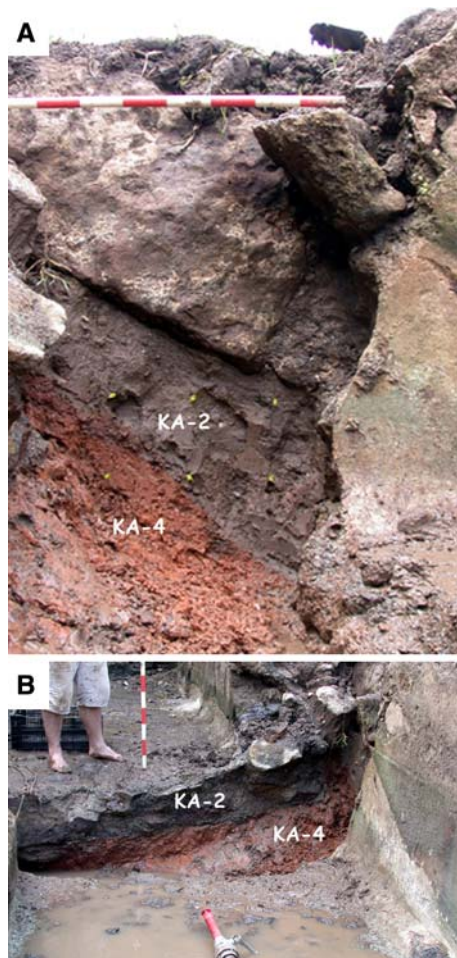
### 3 Geotechnical investigations

Field observations reveal that the basic conditions for slope instability exist in the studied area (i.e., steep slope, weak geological material, high water level). Thus, it is apparent that the observed offset in the water pool, described above, is the result of a landslide. In this section, we study the stability of the slope the water pool is founded on and analyze whether the slope instability (if any) is static or dynamic (i.e., triggered by earthquake). We use air-photo derived DEM and field survey to map the landslide geometry and auger drilling, a few meters into the slide, for soil sampling. The samples are used to evaluate the mechanical properties of the soils.

The angle of internal friction and cohesion of the brown soil (KA-2), the reddish paleosol (KA-4), and the gray palesol (KA-5) were evaluated at the Geological Survey of Israel geotechnical lab, using Direct Shear Test apparatus (ESBL type EL26-2114). The shear-box horizontal dimensions are 10 cm x 10 cm with 2.5 cm depth (type EL26-2197). Tests were performed under undrained consolidated settings (standard BS-1377) to simulate dynamic conditions (Newmark 1965), at normal loads of 50, 100, and 150 kN and shearing speed of 0.59 mm/min. We also measured water content and unit weight for each sample.

Six disturbed (i.e., collected in the field and cast into the shearing box) samples from each unit (KA-2, KA-4, KA-5) were tested, two duplicates under each normal load.

**Fig. 6 a and b** An exploratory trench excavated in the gap between the 2 sections of the pool exposes a red, clay-rich layer of baked fossil soil (KA-4). The clay acts as aquiclude (impermeable layer) of the spring source. Brown clay soil (KA-2) overlies the red clay, and a steep incline to the right (the fallen block of the slide). The contact of the red clay with the brown soil above it shows no signs of discontinuity or discrete dislocation. Rather, its incline suggests a continuous shearing of the clay. Above the brown clay a part of the tilted floor is clearly seen. Distance between the yellow markers: 20 cm



Summary of the results is presented in Table 2. Loading curves of the samples include 3 stages (Fig. 7a): Linear stage, at a shear strain of less than 0.01, where shear strain increases linearly with load; Transition stage, at about 0.01 to 0.06 strain, where sample yield and strain soften; Plastic stage, at strain larger than 0.06, where shear strain increases with almost no increasing stresses (through-going fault develop). Shear stresses at the transition from stage 2 to stage 3 were used to calculate angle of internal friction ( $\phi$ ) and cohesion (C) in a Mohr-Coulomb space (Fig. 7b). For the reddish paleosol (KA-4), in which slope failure developed,  $C = 4.0 \text{ kN/m}^2$  and  $\phi = 31^\circ$  (Table 2). These values are typical to sandy material, as expected considering the grain size analysis (Fig. 3). Angle of internal friction of KA-2 and KA-5 are similar to KA-4 and the cohesion is higher. These cohesion values are in favor of SC types soils rather than SM. Water content measured before the test reflects field natural conditions (Table 2).

The data are used to create a 2-D model of the slope, using the Slope/W<sup>TM</sup> software for slope stability analysis (Fig. 2c). The topographic profile perpendicular to the slope of the landslide area is used for creating the model outline. The model contains 4 units: basalt cliffs above the landslide area (rock), brown soil cover of the basalt where the slope is

**Table 2** Summary of geotechnical data

Sample	Unit weight (kN/m <sup>3</sup> )	Test #	Load (kN)	Water content (% wt)	Peak stress (kN/m <sup>2</sup> )	C (kN/m <sup>2</sup> )	$\varphi$ (°)
KA-2	21.6	1	50	28.0	51.6		
		2			47.4		
		3	100		80.5	18.9	32
		4			81.2		
		5	150		110.9		
		6			111.3		
KA-4	20.8	7	50	23.8	32.1		
		8			33.3		
		9	100		68.7	4.0	31
		10			63.3		
		11	150		91.6		
		12			93.2		
KA-5	16.7	13	50	35.1	45.9		
		14			47.2		
		15	100		75.7	20.4	29
		16			81.5		
		17	150		99.5		
		18			104.0		

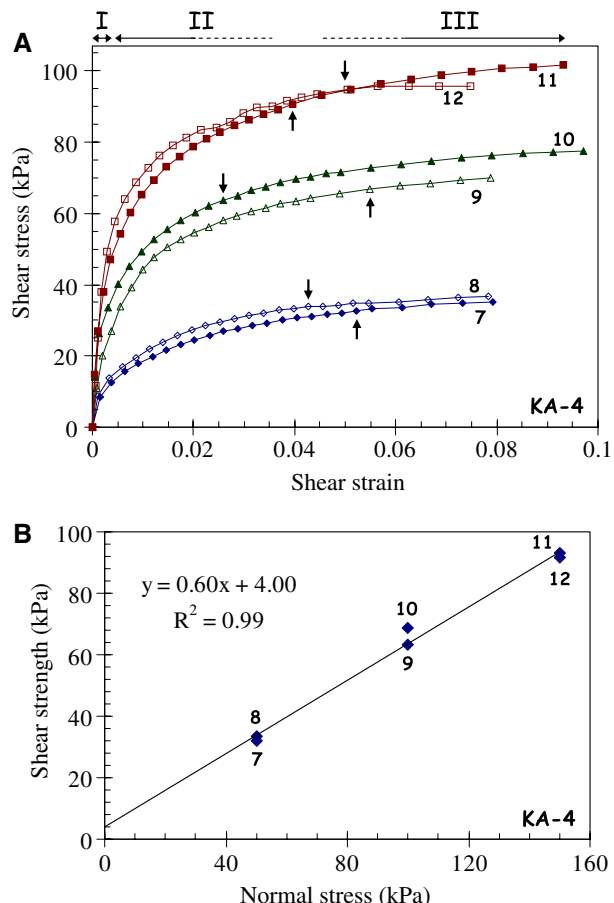
gentler (KA-2), reddish paleosol layer of the spring (KA-4), and a layer below the reddish paleosol that is the gray paleosol (KA-5). The soil mechanical properties are provided for both the brown soil and the reddish paleosol, and their thickness is constrained in part by the auger drilling and in part by geological mapping. Modeling the lowest layer as rock or paleosol does not change the model results due to the relative weakness of the reddish paleosol, so for simplicity the lowest layer is modeled as rock. The water table is set to several levels between the level of the reddish paleosol (the spring's aquifer—lowest possible level) and the level of the topography, assumed to be the highest possible level.

We use two methods of moment equilibrium to compute the stability of the studied slope: the ordinary or “Fellenius method” (Fellenius 1936) and the “modified Bishop method” (Bishop 1955). Both methods belong to a group of methods called “methods of slices,” in which for enabling accurate stability calculations, the analyzed landslide is divided to vertical parallel slices. A possible circular slip surface is assumed, and the driving and resisting moments are computed in each slice in order to determine the Factor of Safety (FS) against sliding. The FS is defined as the sum of resisting moments  $M_r$  (in all slices comprising the landslide) divided by the sum of the driving moments  $M_d$  (in all slices),  $FS = \sum M_r / \sum M_d$ . If the  $FS > 1$  then the slope is considered stable. In the Bishop method the inter-slices vertical shear forces are incorporated into the calculation, giving more conservative values for the FS.

### 3.1 Static analysis

Static FS analysis evaluates the stability of a slope under gravitational forces. Jibson and Keefer (1993) showed that the FS computed from undrained soil parameters do not differ

**Fig. 7** Mechanical properties of the reddish paleosol (KA-4). **a** Shear stress-strain curves for the three different normal loads tested (marked are the test numbers as they appear in Table 2): diamonds, triangle, and squares are normal loads of 50, 100, and 150 kN, respectively (open and close symbols mark the two duplicate tests done under each normal load). The loading path shows similar stages in samples KA-2 and KA-5. Small vertical arrows mark the turnover between stage II and III for each test. **b** Mohr-Coulomb space showing evaluated mechanical properties (plotted for each test are shear strength at the turnover between stage II and III and normal load)



much from the drained FS values, and if it did, the undrained FS values were generally lower. Consequently, using the undrained soil parameters for the static analysis leads to underestimation of the static FS, which is a conservative assumption. If the FS computed from undrained soil parameters clearly indicates that failure in aseismic conditions is highly unlikely, such as in our model, then it should be true for a FS computed from drained soil parameters. Another reason for using undrained soil parameters to calculate the FS are the high values of water content in the samples.

Table 3 summarizes the FS values calculated for several scenarios. The lowest value of the FS obtained from the model is 2.05, where we assume the highest water table. Hence, we conclude that the site is stable under aseismic conditions and that the damage to the pool could not have been caused by gravitational forces alone, even with the driving effect of water from the nearby spring. Therefore, any instability and consequential damage must have been a result of ground shaking due to an earthquake.

### 3.2 Dynamic analysis

We use the Newmark displacement method (Jibson 2007; Jibson et al. 2000; Newmark 1965) to evaluate the slope stability during an earthquake. This method calculates the

**Table 3** The results of the analysis in the Slope/W modeling software for several cases and methods

Case	Ordinary		Bishop	
	FS	a <sub>c</sub>	FS	a <sub>c</sub>
Highest water table	2.05	0.36	2.288	0.44
High water table	2.297	0.44	2.562	0.53
Middle water table	2.869	0.64	3.117	0.72
Low water table	3.026	0.69	3.281	0.78
$\varphi - 1^\circ$	2.797	0.61	3.037	0.70
$\varphi + 1^\circ$	2.942	0.66	3.199	0.75
Unit weight -0.5 %wt	2.889	0.65	3.138	0.73
Unit weight +0.5 %wt	2.856	0.63	3.104	0.72
Cohesion -2 kN/m <sup>2</sup>	2.76	0.60	3.006	0.69
Cohesion +2 kN/m <sup>2</sup>	2.977	0.68	3.229	0.76

The critical acceleration  $a_c$  is calculated from the FS and the slope angle (Eq. 1). The first 4 cases are for different water table levels. The other cases are for measuring the effects of variations in the soil mechanical properties in the middle water table case.  $\phi$ —the angle of internal friction

cumulative permanent displacement (Newmark displacement,  $D_N$ , in centimeters) of a rigid friction block relative to its base as subjected to the effects of the earthquake acceleration–time history. Practically, those acceleration–time history portions that exceed the critical acceleration of the modeled slope are integrated twice to obtain the cumulative displacement history of the block. The critical acceleration,  $a_c$ , is defined as the acceleration required for overcoming the frictional resistance and initiating sliding. The critical acceleration (in units of gravity,  $1\text{ g} = 9.8\text{ m/s}^2$ ) is a function of the static factor of safety (FS) and the landslide geometry (Newmark 1965):

$$a_c = (\text{FS} - 1) \sin \beta \quad (1)$$

where  $\beta$  is the angle between the vertical and the line connecting the center of mass and the center of rotation (e.g., Jibson and Keefer 1993). We found  $\beta$  to be  $20^\circ$  in our model.

The lack of a strong motion record for the Sea of Galilee area, where the last strong earthquake occurred in 1837, prevents us from using the rigorous analysis of double integration of a strong motion record from a nearby locality. Jibson and Keefer (1993) and Jibson et al. (2000) suggested an alternative for the calculation of the Newmark Displacement ( $D_N$ ) as a assessment for slope stability, using an empirical relationship between it and the critical acceleration and the Arias intensity  $I\alpha$  (Arias 1970), a quantity that correlates with peak ground acceleration and duration of shaking of an earthquake:

$$\log D_N = 1.521 \log I\alpha - 1.993 \log a_c - 1.546 \quad (2)$$

Jibson et al. (2000) derived this empirical law from over 200 strong-motion records from Southern California. Because of absence of recorded strong events from the DST we use the relation for Southern California, assuming that the similarity of seismic behavior between two transform plate boundaries is significant. A similar approach was also used by Jibson and Keefer (1993) for the New-Madrid zone and by Katz and Crouvi (2007) for the DST region.

Arias intensity,  $I\alpha$ , can be related by empirical relation to earthquake moment magnitude ( $M_w$ ) and the distance from epicenter in km (R) (Jibson and Keefer 1993). The  $I\alpha$  for the Dead Sea area is (Katz and Crouvi 2007):

$$\log I\alpha = 1.2M_w - 2.2 \log R - 4.9 \quad (3)$$

The resultant Newmark displacement does not necessarily predict the physical landslide displacement in the field; rather, it is a useful index of how a slope is likely to perform during seismic shaking. The user has to judge the significance of the displacement. Following Jibson et al. (2000), we choose the  $D_N$  to be either 5 or 10 cm for the critical displacement that would cause the slope to fail, where the larger value is more conservative and therefore preferable.

We analyze the earthquake magnitude needed to cause slope instability as a function of distance from the epicenter for both  $D_N$  values. The lowest critical acceleration provides us with the upper bound of distance as a function of magnitude, and imposes constraints on the location of the epicenter.

Figure 8 shows the distance vs. magnitude results of the Newmark analysis for the minimum, maximum, and mean critical acceleration values, compared to the maximum distance of landslides from epicenter and surface rupture (Keefer 1984). The results for all models are summarized in Table 4. The lowest critical acceleration value occurs in the case of the highest water table. The results show that even for an event with epicentral or rupture distance of 5 km from Umm-El-Qanatir, the earthquake moment magnitude needed to activate the sliding is at least 6, more likely close to 6.5. Using the known location of the slide, we can draw radii of magnitudes, as shown in Fig. 9, for the lowest critical acceleration ( $a_c = 0.36$ ). It is evident that the site is about 15 km away from the closest possible source of strong earthquake, although smaller events are apparent in closer proximity in the present day seismicity. At a distance of 15 km the magnitude needed to overcome slope strength and trigger the landslide is at least 7. From this and from the aforementioned archaeological evidence, we conclude that Umm-El-Qanatir was hit by an  $M_w \geq 7$  close earthquake in the mid 8th century.

**Fig. 8** Newmark Displacement (in cm) as a function of Moment magnitude and distance from epicenter (in km) for several critical acceleration values:  $a_c = 0.36$  (red line), the lowest acceleration calculated from the FS values for the slope failure;  $a_c = 0.78$  (black dotted line), the highest acceleration calculated;  $a_c = 0.64$  (blue dashed line), the mean value; dashed green line and black line mark the maximum distance from epicenter and fault rupture where landslides occur (Keefer 1984), respectively

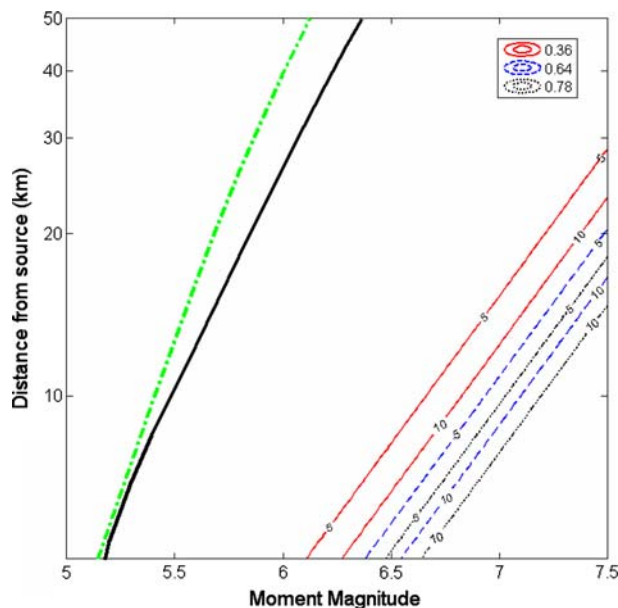
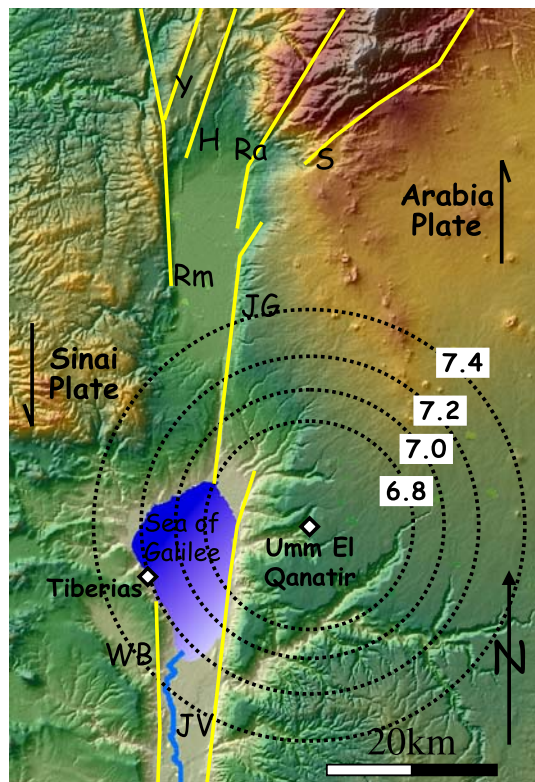


**Table 4** Results of the Newmark analysis for the minimum, maximum, and mean values of the critical acceleration

Newmark displacement $D_N$	5 cm			10 cm		
	Critical acceleration $a_c$	0.36 g	0.64 g	0.78 g	0.36 g	0.64 g
Distance (km)						
Magnitude						
6.2	5.6	4.0	3.5	4.5	3.2	2.9
6.4	7.2	5.1	4.5	5.8	4.2	3.7
6.6	9.2	6.6	5.8	7.5	5.3	4.7
6.8	11.9	8.4	7.5	9.7	6.9	6.1
7.0	15.3	10.9	9.6	12.4	8.8	7.8
7.2	19.7	13.9	12.4	16.0	11.3	10.1
7.4	25.3	17.9	15.9	20.5	14.6	13.0

**Fig. 9** Circles showing maximal distance from Umm-El-Qanatir of earthquakes that can trigger slope failure for a given magnitude ( $M_W$ ). For this map,  $a_c = 0.36$  and  $D_N = 5$  cm, the most conservative values that give the largest distances (see Table 4). Active faults are yellow (names of faults as appear in Fig. 1). Shaded relief from Hall (1994)



#### 4 Discussion

Umm-El-Qanatir exhibits earthquake damage that is constrained by archaeological artifacts to the mid 8th century or later. Moreover, a strong and near-by earthquake triggered a landslide that displaced the spring area. The DST, less than 15 km west of the site, is the only

fault capable of producing magnitude 6 and larger earthquakes. Several strong earthquakes that are reported in historical records since the mid 8th century may be candidates for the triggering or reactivation of the slide (listed in the Introduction). The key to identifying the correct event is the dating. The slide is not dated directly; therefore, we cannot rule out the possibility that it was reactivated in one or more of those events. However, since the village of Umm-El-Qanatir was abandoned immediately after 749 CE and no Abbasid period or later artifacts are found in the ruins of Umm-El-Qanatir, we argue that it was abandoned because of the severe damage to the spring area, which was an important part of the villager's economy. Hence, most likely the 749 CE earthquake triggered the slide.

Our Newmark analysis related to the 749 CE event yields reasonable results, as the comparison with the data of landslide distances from the earthquake sources shows (Fig. 8). The magnitude versus distance results are within the range of plausible values compared with known worldwide events, supporting the approach of using the empirical relations intensity-displacement-magnitude-distance. Even when considering the most conservative values of critical acceleration and Newmark displacement, a strong earthquake ( $M_w = 7.4$ ) would have to occur within  $\sim 25$  km radius of Umm-El-Qanatir in order to cause slope failure (Fig. 9).

Our analysis does not consider topography effects directly. Davis and West (1975) report stronger topography-related amplification on ridge-tops and weaker in valley floors. A significant topographic effect occurs when the wavelength of the seismic wave is the same as the length of the landform, and the greatest amplification of ground acceleration occurs when nearly horizontal waves traverse canyon topography where the distance between the canyon walls is less than or equal to the wavelength. Since Umm-El-Qanatir sits on the top of the river gorge, amplification effect probably makes it more susceptible to landslides due to amplification of ground motions. However, the influence of topography on acceleration and induced landslides has been mainly observed empirically, and there are no general models for quantifying site amplification due to topography effects. Moreover, the overall influence on ground motion in complex topography cannot be easily predicted. Therefore, modeling the topographic effect is beyond the scope of this paper. By making conservative choices about the Newmark Displacement and the Factor of Safety, we assume that the topographic effect is indirectly partially compensated for.

## 5 Conclusions

Historical records and archaeological observations in Umm-El-Qanatir show that the site was hit by at least one damaging earthquake in mid 8th century before the Abbasid period. Damage to archaeological structures, the morphology, and the geology of the site show that the latter earthquake was associated with the studied landslide. An offset water pool provides a measure of the slip associated with the landslide. We combine the slip with measured mechanical properties of the rock units in a model of a landslide, which relates the slip to acceleration and then to magnitude-distance. The result of this analysis imposes constraints on the range of possible magnitude-distance of the earthquake from Umm-El-Qanatir.

We conclude that if the 749 CE earthquake triggered the landslide, then the magnitude of the earthquake was at least 7.0 at a distance of up to 15 km from Umm-El-Qanatir (Fig. 9). For large events, which rupture the whole seismogenic zone, the distribution of the associated strong motion usually follows the rupture, so that this distance can be considered as distance from the fault rupture zone (Keefer 2002).

**Acknowledgments** We are grateful to all the people who worked in the archeological excavations—Noam Aharoni, Tuvia Ka’atabi, and Hanoch Tal. We thank Mor Kanari and Boaz Gatenio for their assistance in the field. Part of the study was supported by an Israel Science Foundation grant 12/03 to SM.

## References

- Ambraseys NN (2005) The seismic activity in Syria and Palestine during the Middle of the 8th century; an amalgamation of historical earthquakes. *J Seismol* 9(1):115–125. doi:[10.1007/s10950-005-7743-2](https://doi.org/10.1007/s10950-005-7743-2)
- Amiran DHK, Arie E, Turcotte T (1994) Earthquakes in Israel and adjacent areas: Macroseismic observations since 100 B.C.E. *Isr Explor J* 44:260–305
- Arias A (1970) A measure of earthquake intensity. In: Hansen RJ (ed) *Seismic design for nuclear power plants*. Massachusetts Institute of Technology Press, Cambridge, pp 438–483
- ASTM (1985) Classification of soils for engineering purposes. In: Annual book of ASTM standards. American Society for Testing and Materials, pp 395–408
- Bartov Y, Sneh A, Fleischer L, Arad V, Rosensaft M (2002) Map of potentially active faults in Israel. Geological Survey of Israel report GSI/29/02, Jerusalem
- Begin BZ, Steinberg DM, Ichinose GA, Marco S (2005) A 40,000 years unchanging of the seismic regime in the Dead Sea rift. *Geology* 33(4):257–260. doi:[10.1130/G21115.1](https://doi.org/10.1130/G21115.1)
- Bishop AW (1955) The use of the slip circle in the stability analysis of slopes. *Geotechnique* 5:7–17
- Daéron M, Klinger Y, Tapponnier P, Elias A, Jacques E, Sursock A (2005) Sources of the large AD 1202 and 1759 Near East earthquakes. *Geology* 33(7):529–532. doi:[10.1130/G21352.1](https://doi.org/10.1130/G21352.1)
- Davis LL, West LR (1975) A preliminary evaluation of the effects of topography on ground motion. *Calif Div Mines Geol Bull* 196:305–312
- Ellenblum R, Marco S, Agnon A, Rockwell T, Boas A (1998) Crusader castle torn apart by earthquake at dawn, 20 May 1202. *Geology* 26(4):303–306. doi:[10.1130/0091-7613\(1998\)026<0303:CCTABE>2.3.CO;2](https://doi.org/10.1130/0091-7613(1998)026<0303:CCTABE>2.3.CO;2)
- Fellenius W (1936) Calculations of the stability of earth dams. *Trans second congress of large dams*, vol 4, pp 445–463, Washington
- Freund R, Zak I, Garfunkel Z (1968) Age and rate of the sinistral movement along the Dead Sea Rift. *Nature* 220:253–255. doi:[10.1038/220253a0](https://doi.org/10.1038/220253a0)
- Garfunkel Z (1981) Internal structure of the Dead Sea leaky transform (rift) in relation to plate kinematics. *Tectonophysics* 80:81–108. doi:[10.1016/0040-1951\(81\)90143-8](https://doi.org/10.1016/0040-1951(81)90143-8)
- Guidoboni E, Comastri A (2005) Catalogue of Earthquakes and Tsunamis in the Mediterranean Area from the 11th to the 15th century. Istituto Nazionale di Geofisica, Bologna, p 1037
- Guidoboni E, Comastri A, Traina G (1994) Catalogue of Ancient Earthquakes in the Mediterranean Area up to the 10th century. Istituto Nazionale di Geofisica, Bologna, p 504
- Hall JK (1994) Digital shaded-relief map of Israel and environs 1:500,000. Israel Geological Survey
- Jibson RW (2007) Regression models for estimating coseismic landslide displacement. *Eng Geol* 91(2–4): 209–218. doi:[10.1016/j.enggeo.2007.01.013](https://doi.org/10.1016/j.enggeo.2007.01.013)
- Jibson RW, Keefer DK (1993) Analysis of the seismic origin of landslides—examples from the New-Madrid Seismic Zone. *Geol Soc Am Bull* 105(4):521–536. doi:[10.1130/0016-7606\(1993\)105<0521:AOTSOO>2.3.CO;2](https://doi.org/10.1130/0016-7606(1993)105<0521:AOTSOO>2.3.CO;2)
- Jibson RW, Harp EL, Michael JA (2000) A method for producing digital probabilistic seismic landslide hazard maps. *Eng Geol* 58:271–289. doi:[10.1016/S0013-7952\(00\)00039-9](https://doi.org/10.1016/S0013-7952(00)00039-9)
- Karcz I (2004) Implications of some early Jewish sources for estimates of earthquake hazard in the Holy Land. *Ann Geophys* 47(2–3):759–792
- Katz O, Crouvi O (2007) The geotechnical effects of long human habitation (2000 < years): Earthquake induced landslide hazard in the city of Zefat, northern Israel. *Eng Geol* 95(3–4):57–78. doi:[10.1016/j.enggeo.2007.07.008](https://doi.org/10.1016/j.enggeo.2007.07.008)
- Keefer DK (1984) Landslides caused by earthquakes. *Geol Soc Am Bull* 95:406–421. doi:[10.1130/0016-7606\(1984\)95<406:LCBE>2.0.CO;2](https://doi.org/10.1130/0016-7606(1984)95<406:LCBE>2.0.CO;2)
- Keefer DK (2002) Investigating landslides caused by earthquakes—a historical review. *Surv Geophys* 23(6):473–510. doi:[10.1023/A:1021274710840](https://doi.org/10.1023/A:1021274710840)
- Kohl H, Watzinger C (1916) Antike Synagogen in Galilaea. J. C. Hinrichs, Leipzig
- Marco S (2008) Recognition of earthquake-related damage in archaeological sites: examples from the Dead Sea fault zone. *Tectonophysics* 453:148–156. doi:[10.1016/j.tecto.2007.04.011](https://doi.org/10.1016/j.tecto.2007.04.011)
- Marco S, Hartal M, Hazan N, Lev L, Stein M (2003) Archaeology, history, and geology of the A.D. 749 earthquake, Dead Sea Transform. *Geology* 31(8):665–668. doi:[10.1130/G19516.19511](https://doi.org/10.1130/G19516.19511)

- 
- Marco S, Rockwell TK, Heimann A, Frieslander U, Agnon A (2005) Late Holocene slip of the Dead Sea Transform revealed in 3D palaeoseismic trenches on the Jordan Gorge segment. *Earth Planet Sci Lett* 234(1–2):189–205. doi:[10.1016/j.epsl.2005.01.017](https://doi.org/10.1016/j.epsl.2005.01.017)
- Michelson H (1979) The geology and paleogeography of the Golan Heights. In: Tel Aviv University, Tel Aviv, p 163
- Newmark NM (1965) Effects of earthquakes on dams and embankments. *Geotechnique* 15:139–160
- Oliphant L (1886) Haifa. In: Dana CA (ed) Life in modern Palestine. W. Blackwood, Edinburgh, p 369
- Reches Z, Hoexter DF (1981) Holocene seismic and tectonic activity in the Dead Sea area. *Tectonophysics* 80:235–254. doi:[10.1016/0040-1951\(81\)90151-7](https://doi.org/10.1016/0040-1951(81)90151-7)
- Sbeinati MR, Darawcheh R, Mouty M (2005) The historical earthquakes of Syria: an analysis of large and moderate earthquakes from 1365 B.C. to 1900 A.D. *Ann Geophys* 48(3):347–435
- Schumacher G (1886) Across the Jordan: being an exploration and survey of part of Hauran and Jaulan. R. Bentley, London, p 342
- Segal A, Mlynarczyk J, Burdajewicz M, Schuler M, Eisenberg M (2003) Hippos-Sussita: fourth season of excavations, June–July 2003. In: Zinman Institute of Archaeology, Haifa University, Haifa, p 101